NANO LETTERS

pubs.acs.org/NanoLett

Letter

Uncovering Topological Edge States in Twisted Bilayer Graphene

Matthieu Fortin-Deschênes,* Rui Pu, Yan-Feng Zhou,* Chao Ma, Patrick Cheung, Kenji Watanabe, Takashi Taniguchi, Fan Zhang, Xu Du,* and Fengnian Xia

Cite This: *Nano Lett.* 2022, 22, 6186−6193

Read Online

ACCESS | Metrics & More | Article Recommendations | Supporting Information

ABSTRACT: Twisted bilayer graphene (t-BLG) has recently been introduced as a rich physical platform displaying flat electronic bands, strongly correlated states, and unconventional superconductivity. Studies have hinted at an unusual Z_2 topology of the moiré Dirac bands of t-BLG. However, direct experimental evidence of this moiré band topology and associated edge states is still lacking. Herein, using superconducting quantum interferometry, we reconstructed the spatial supercurrent distribution in t-BLG Josephson junctions and revealed the presence of edge states located in the superlattice band gaps. The absence of edge conduction in high resistance regions just outside the superlattice band gap confirms that the edge transport originates from the filling of electronic states located inside the band gap and further allows us to exclude several other edge conduction mechanisms. These results confirm the unusual moiré band topology of twisted bilayer graphene and will stimulate further research to explore its consequences.

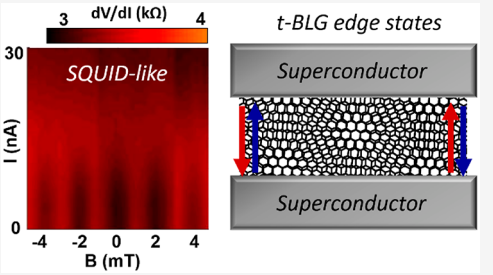

KEYWORDS: *two-dimensional materials, twisted bilayer graphene, topology, edge states, Josephson junctions, moiré*

Stacking two two-dimensional (2D) lattices with a relative twist angle or a slight lattice mismatch has been shown to extend the potential of 2D materials by generating a larger (quasi-) periodic lattice, called a moiré pattern (Figure 1a).[1−5] For instance, the moiré pattern has been found to both localize and tune interlayer excitons in transition metal dichalcogenides heterostructures.[6−10] In twisted bilayer graphene (t-BLG), near the magic angle of 1.05°, hybridization and interference of the Dirac cones of the two layers can lead to a drastic reduction of the electronic bandwidth of the lowest moiré bands and to the formation of superlattice (SL) band gaps[11,12] (Figure 1b). These flat mini-bands give rise to various correlated electronic phases such as unconventional superconductivity.[13−17] Recently, the nontrivial band topology of t-BLG has attracted a lot of attention.[18−27] In fact, the moiré Dirac bands are topologically characterized by two nontrivial Z_2 invariants.[25] Moreover, theoretical analyses suggest that t-BLG could be an experimentally accessible second-order topological insulator hosting gapped edge states[25] and in-gap corner states.[19,24,26] Transport and scanning-tunnelling microscopy studies of Bernal-stacked and minimally twisted t-BLG revealed the presence of valley-projected helical 1D states at the boundaries between AB and BA stacked domains.[28−32] On the other hand, nonlocal transport measurements point toward the existence of edge states within the SL band gaps of t-BLG near and above the magic angle.[25] Nonetheless, direct observations of the edge states emerging from of the nontrival moiré band topology are critically needed.

Herein, using superconducting quantum interferometry (SQI) we reconstruct the supercurrent spatial distribution in t-BLG Josephson junctions (JJs).[33,34] By tuning the position of the Fermi level, we demonstrate the redistribution of the conduction channels from the bulk to the edges of the JJs as the Fermi level enters the SL band gap. Edge conduction mechanisms unrelated to the moiré bands, such as conduction by trivial dangling bond states, are excluded because of the absence of edge current in high-resistance regions just outside the SL band gaps. Furthermore, we identify an anomalous periodicity in the magnetic flux dependence of the supercurrent at fillings between approximately ±4−5 electrons per moiré unit cell in devices with high twist angle homogeneity.

t-BLG heterostructures (twist angle of 1.2−1.8°) encapsulated by hBN were fabricated using the tear and stack method[3,35] (Figure 1c). Extremely clean interfaces between the layers were produced by squeezing contaminants out of the heterostructures with an atomic force microscopy tip.[36] Edge contacts to superconducting molybdenum−rhenium (MoRe) were used to define MoRe/t-BLG/MoRe JJs with width (W) of 2−3 μm and length (L) of 100−300 nm (Figure 1d, e). The carrier concentration (n) in t-BLG is controlled by a global silicon back gate (Figure 1d). The two-terminal resistance of device 1 (D1) (W = 3 μm, L = 100 nm, twist angle of 1.74°), measured at 80 K, shows the insulating states at $n = \pm 7.0 \times 10^{12}$ cm^{-2}, corresponding to fillings of ±4e per moiré unit cell

Received: April 13, 2022
Revised: July 19, 2022
Published: July 28, 2022

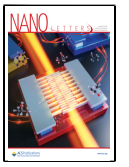

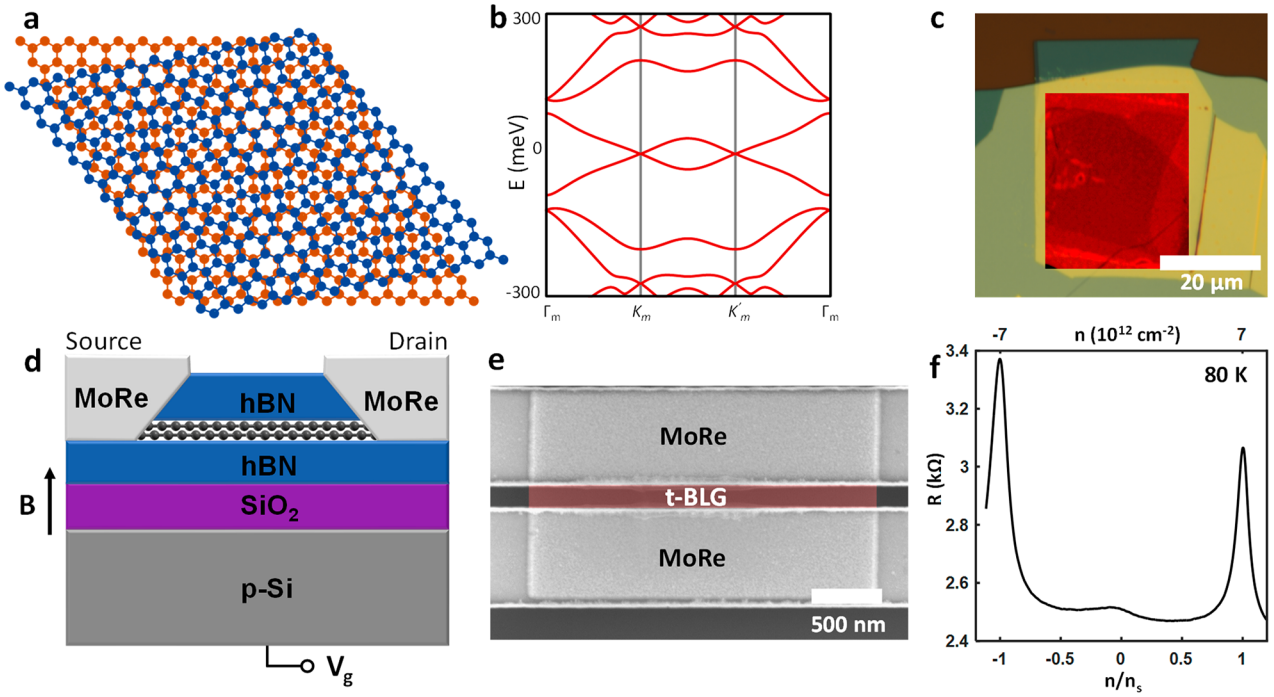

Figure 1. (a) Schematics of the moiré pattern formed by twisting two graphene lattices. (b) Band structure of t-BLG with a twist angle of 1.74°. (c) Optical microscopy image of t-BLG encapsulated by hBN. The contrast of the t-BLG region is enhanced for visibility. (d) Schematics of the t-BLG JJs used for superconducting quantum interference measurements. MoRe edge contacts are made to the t-BLG and a variable perpendicular magnetic field is applied. The carrier concentration is controlled by the silicon back gate. (e) Scanning-electron microscopy image of a MoRe/t-BLG/MoRe JJ. The t-BLG is false-colored in red. (f) Two-terminal resistance as a function of carrier concentration for device D1 at 80 K. The top horizontal axis indicates the absolute carrier concentration, and the bottom horizontal axis indicates the carrier concentration with respect to full filling of n_s (four electrons per moiré unit cell).

($n = n_s$). We note that the high resistance in the metallic state ($n \approx 0.5n_s$) is due to the finite resistance (~2.5 kΩ) of the MoRe leads above T_c.[37] Nonetheless, the sheet resistance of the JJ associated with the SL peak is $R_s \approx 18$ kΩ/□ (resistance difference between the insulating and conducting states), which indicates a high device quality and relatively good twist angle homogeneity (Figure S1). This is critical for the observation of the edge states, as impurities or twist-angle inhomogeneities can easily shunt the device because of its ultrashort length.

We now turn our attention to the behavior of the t-BLG JJ at T = 300 mK. Applying a perpendicular magnetic field B introduces a position-dependent phase across the device, thus resulting in an interference pattern of the critical current of the Josephson junction $I_c(B)$:[33,34]

$$I_c(B) = \left| \int_{-\infty}^{\infty} J_s(x) \exp[2\pi i(L + 2\lambda_L)Bx/\Phi_0]dx \right| \quad (1)$$

where J_s is the supercurrent density, λ_L is the effective London penetration depth of the magnetic field in the superconducting MoRe electrodes (accounting for flux focusing[34]), and $\Phi_0 = h/2e$ is the magnetic flux quantum. This method allows for the reconstruction of the supercurrent density in 2D materials JJs by taking the inverse Fourier transform of eq 1.[34,38,39] Moreover, the interference pattern originating from the magnetic flux enclosed by the JJ (Φ) can be used to readily identify the dominating conducting channels. In fact, a uniform current distribution across the junction leads to a Fraunhofer-like interference pattern $I_c(B) \sim |\mathrm{sinc}(\pi\Phi/\Phi_0)|$ (Figure 2a), where the amplitude of the lobes (I_c) decays as $1/B$ and the width of the center lobe ($2\Phi_0$) is twice the width of the side lobes (Φ_0). On the other hand, edge conduction leads to a sinusoidal SQUID-like pattern $I_c(B) \sim |\cos(\pi\Phi/\Phi_0)|$ (Figure 2b), where all lobes have a width of Φ_0 and identical amplitude.

The $I_c(B)$ interference patterns at and away from the SL band gap (Figure 2c) are shown in Figure 2d. When the Fermi level is placed outside the gap ($n = 0.32n_s$) or at the Dirac point, Fraunhofer interference patterns are observed (Figure 2d and Figure S2). The width of the center and side lobes are 1.92 and 0.96 mT, and I_c decays as $1/B$. This is reflected in the reconstructed spatial supercurrent distribution (Figure 2e), which is mostly homogeneous along the width of the t-BLG JJ (Figure 2e). Although expected, this homogeneous conduction shows that there are no appreciable current inhomogeneities introduced by uneven contact transparency or length variations along the ultrashort junction, for instance. On the other hand, the interference pattern undergoes significant changes when the Fermi level enters the band gap ($0.96n_s$ and n_s in Figure 2d). There, I_c decreases because of the high resistance. Furthermore, the width of the central lobe reduces to 1.6 mT at $0.96n_s$ and 1.7 mT at n_s. The amplitude of the side lobes remains relatively constant up to at least 10 mT (Figure 2d and Figure S2). Such SQUID-like characteristics suggest edge conduction. Nonetheless, the width and amplitude of the central lobe is still larger than the side lobes, which indicates the presence of residual bulk conduction. Moreover, the side lobes' periodicity is not constant, revealing current inhomogeneities. The supercurrent reconstructions allow to visualize the transition from bulk to edge conduction when the Fermi level approaches n_s (Figure 2e), implying the presence of edge states located inside the band gap. This further strengthen the

https://doi.org/10.1021/acs.nanolett.2c01481
Nano Lett. 2022, 22, 6186−6193

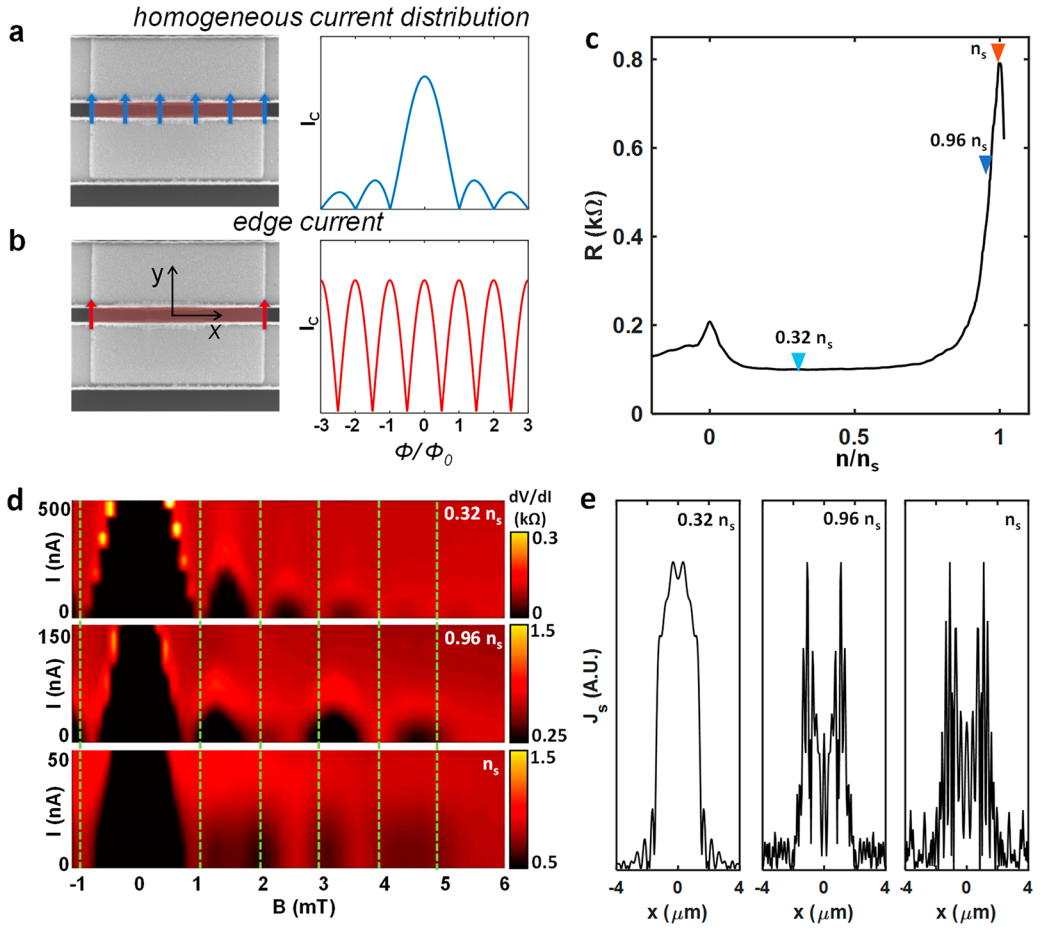

Figure 2. (a) Illustration of homogeneous current flow in a JJ and the resulting Fraunhofer interference pattern. (b) Illustration of edge current flow in a JJ and the resulting SQUID interference pattern. (c) Quasi four-terminal resistance as a function of carrier concentration at 6 K using 1 μA AC excitation to avoid supercurrent for device D1. The colored triangles indicate the carrier concentrations for the interference patterns in d. (d) Interference patterns at carrier concentrations below and at the superlattice band gap (300 mK). The dashed lines indicate the positions of the nodes for the Fraunhofer pattern at $0.32n_s$. (e) Reconstructed supercurrent distributions for the interference patterns in d.

hypothesis of the nontrivial topology of the moiré bands of t-BLG.[19,24−26] Nonetheless, the residual bulk conduction and the supercurrent inhomogeneities partially shunt the edge conduction. These imperfections likely originate from slight twist angle inhomogeneities, which result in an uneven position of the band gap inside the JJ.

To further understand the impact of twist angle inhomogeneity on the $I_c(B)$ dependence, we looked at the behavior of other t-BLG JJs with very high sheet resistance in the insulating state. Their large and narrow resistance peaks at the SL gap (Figure S1) suggest a uniform distribution of the location of the gap and thus high twist angle homogeneity. The two-terminal resistance of device 2 (D2) (W = 2 μm, L = 100 nm, twist angle of 1.41°) as a function of n at 80 K is shown in Figure 3a. The sheet resistance associated with the SL peak (R_s > 50 kΩ/□) is about three times larger than for D1. Although the fwhm of the SL peak (1.00×10^{12} cm^{-2}) is larger for D2 than for D1 (0.81×10^{12} cm^{-2}), the broadening on the valence band side (left of the electron side peak) is due to the smaller DOS and lower Fermi velocity associated with the smaller twist angle. However, the narrow width of the conduction band side of the peak (0.24×10^{12} cm^{-2} half width) is consistent with a homogeneous twist angle. We note that the electron and hole-side SL peaks are not exactly symmetrical, but their R_s and width correlate with each other and are expected to be good indicators of twist angle homogeneity. The differential resistance (dV/dI) as a function of the DC bias (V_b) at T = 300 mK and B = 0 is plotted in Figure 3b. At filling of 1.08 and $1.05n_s$, dV/dI vanishes at V_b = 0 and supercurrent flows through the JJ. However, as the Fermi level approaches the gap (n = $0.99n_s$), I_c decreases because of the large normal state resistance R_N (~3 kΩ) and thermal fluctuations thus lead to a finite dV/dI, even at small current. Nonetheless, the clear drop of the resistance at V_b = 0 can still be attributed to the Josephson effect. This allows for the measurement of SQI patterns.

The $I_c(B)$ interference patterns and current densities at $1.39n_s$ and $0.99n_s$ for D2 are shown in Figure 3c−f and Figure S3. Like D1, $I_c(B)$ has the main characteristics of a Fraunhofer pattern when the Fermi-level is placed outside the SL gap (Figure 3c). I_c decays as B increases and the width of the center lobe (1.40 mT) is approximately twice the width of the side lobes (~0.7 mT). We note some irregularities in the period of the SQI at $1.39n_s$, because of a slightly inhomogeneous current distribution. At full filling, $I_c(B)$ is a pure SQUID-like interference pattern (Figure 3e), with equal center ($B \sim 0$) side lobes width (1.88 mT). Moreover, there is no noticeable decay of the amplitude (I_c) of the lobes with increasing B, consistent with edge-dominated transport without residual bulk conduction. Interestingly, the period of

https://doi.org/10.1021/acs.nanolett.2c01481
Nano Lett. 2022, 22, 6186−6193

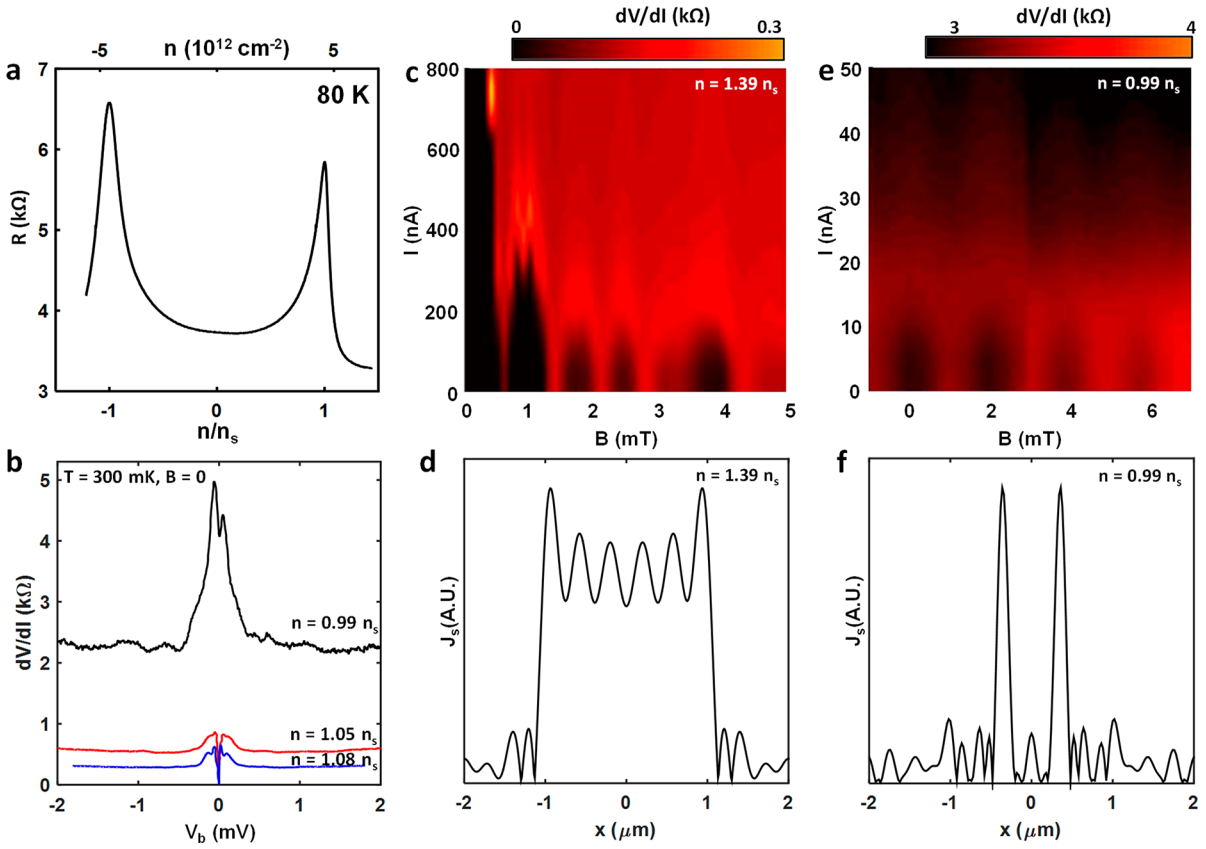

Figure 3. (a) Two-terminal resistance as a function of carrier concentration for device D2 at 80 K. (b) Differential resistance vs measured DC bias across the t-BLG JJ (D2) at different fillings. (c) dV/dI vs B and I_{DC} showing an imperfect Fraunhofer-like interference pattern at $n = 1.39n_s$ (away from the SL gap). (d) Reconstructed current distribution in the t-BLG JJ at $n = 1.39n_s$ indicating bulk dominated conduction. (e) SQUID-like interference pattern (dV/dI vs B and I_{DC}) at $n = 0.99n_s$ (bottom of the SL gap). (f) Reconstructed supercurrent distribution in the t-BLG JJ at $n = 0.99n_s$ showing two main conduction channels.

the SQUID-like pattern at full filling is 2.7 times larger than the period of the Fraunhofer pattern at $1.39n_s$. This is reflected in the inverse Fourier transform of $I_c(B)$, which yields two main conduction channels (Figure 3f) that appear to be located away from the physical edges of the JJ, because of the increased period. Importantly, the 2.7 ratio is also observed in device 3 (D3), another highly homogeneous device, as detailed in the next section.

The period increase can be caused by either the formation of two (or three) conduction channels spaced by $(1/2.7)W$ or by another phenomenon that influences the period of the interference pattern. However, there is no obvious physical mechanism that would lead to the presence of conduction channels spaced by $(1/2.7)W$, especially considering the reproducibility of the phenomenon in devices with different W and aspect ratios. The increased period at full filling is therefore highly unlikely to originate from such a current distribution. On the other hand, increased periods have been observed in monolayer graphene JJs[40] and other systems.[41−44] In theory, periodicity doubling can originate from various effects such as crossed Andreev reflections,[41,42,45] nonlocal supercurrent,[43] or the presence of Majorana zero modes.[44,46,47] Moreover, having a third conduction channel, located at the center of the junction and having the same conductance as the edge states, would double the period of the SQUID interference pattern.[45] However, even with experimental uncertainty, the period increase in this work is larger than 2, thus making it implausible that these mechanisms are at the origin of the observed 2.7 ratio. Because regular Fraunhofer patterns with consistent periodicities are observed at multiple fillings between and away from the SL gaps, we conclude that the SQUID patterns have an anomalous period, rather than the other way around. Moreover, the estimated periods accounting for flux focusing from the MoRe leads are in good agreement with the measured Fraunhofer periods (Table S1).

In principle, the period is determined by the magnetic flux (area and B) and the charge of the particle carrying the supercurrent. The area can be estimated by $W(L + 2\lambda_L)$, and flux focusing can increase the flux through the effective area. However, these parameters are determined by the device geometry (W and L) and the properties of the superconductor (λ_L) and should not be affected by the carrier concentration in t-BLG. On the other hand, the magnetic field through the junction could be influenced by the presence of a magnetic phase. Although ferromagnetism has been observed in t-BLG at $1/2n_s$[48] and $3/4n_s$,[17] such phases should not emerge at full filling of the moiré bands (i.e., n_s) and are unlikely to be involved in our devices. Finally, a period increase is expected if the supercurrent is carried by quasiparticles with charge smaller than $2e$. Theoretical studies hypothesized that t-BLG could be a second-order topological insulator hosting in-gap fractional corner charges[24,26] of $5/6e$ and $e/2$. The 2.7 increase in period would require a charge of $\sim 3/4e$. Nonetheless, these corner states are not protected and easily passivated, which makes them unlikely to present themselves or dominate over the 1D edge states in our experiment. The reproducibility of the 2.7

https://doi.org/10.1021/acs.nanolett.2c01481
Nano Lett. 2022, 22, 6186−6193

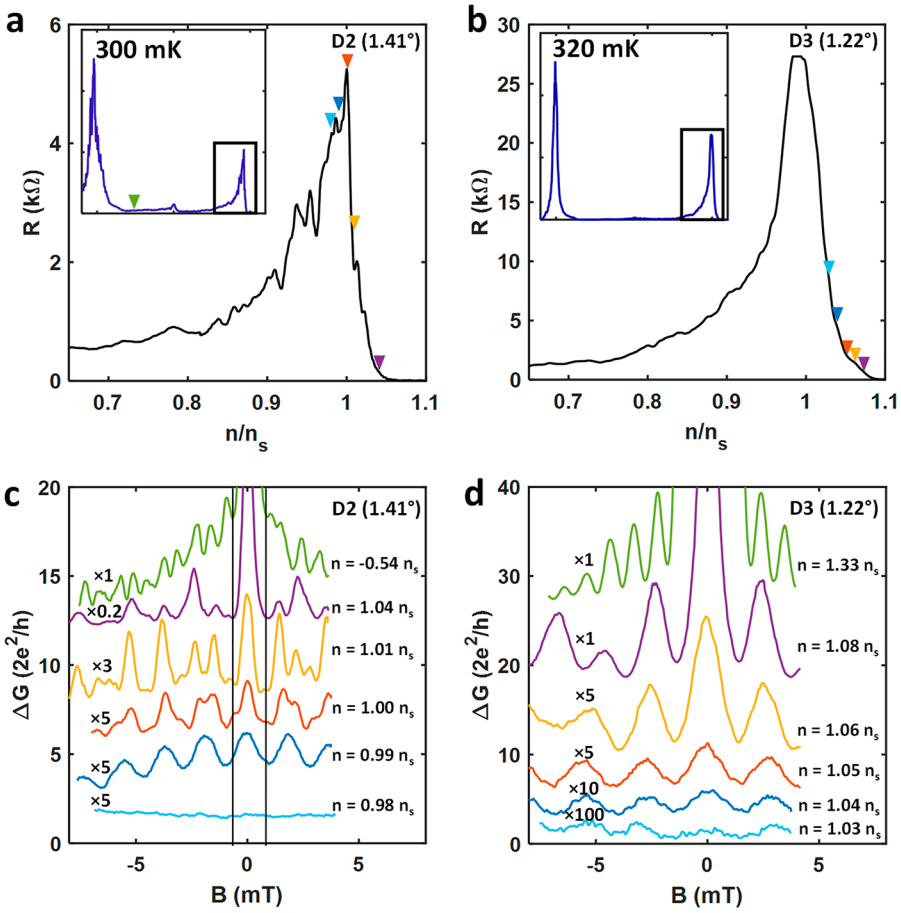

Figure 4. (a) R vs n near the SL band gap for D2, measured at 300 mK. Inset shows the full scan from ($-1.2n_s$ to $1.2n_s$). The colored triangles indicate the carrier concentrations for the data in c. (b) R vs n near the SL band gap for D3, measured at 320 mK. Inset shows the full scan from ($-1.2n_s$ to $1.2n_s$). The colored triangles indicate the carrier concentrations for the data in d. (c) ΔG vs B for carrier concentrations near and away from $n = n_s$ showing the evolution of the supercurrent conduction channels in D2 (300 mK). (d) ΔG vs B for carrier concentrations near and away from $n = n_s$ showing the evolution of the supercurrent conduction channels in D3 (320 mK).

factor in two high-quality devices, and the observation of a similar behavior on the hole side SL gap (Figure S4) suggests that the effect is intrinsic to the band structure of t-BLG. We also note that superconductivity can be induced by the proximity effect on the four t-BLG edges surrounding the channel. If this is the case, resistance oscillations with a period of Φ_0/WL = 10.34 mT would be expected because of the Little-Parks effect,[49] and significant flux focusing could explain the measured period. Further investigation is therefore required to better understand the phenomenon. Nonetheless, the observed behavior at full filling is consistent with edge dominated conduction.

Next, we take a deeper look at the evolution of the SQI patterns at fillings around n_s for the highly homogeneous devices D2 and D3 (Figure 4). D3 has L = 100 nm, W = 2.5 μm, a 1.22° twist angle, and R_s > 60 kΩ/□ in the insulating state at 80 K. The two devices have a similar $R(n)$ behavior at 300 mK (Figure 4a, b). We note the presence of multiple peaks within the SL insulating peak of D2 (Figure 4a), which can be due to universal conductance fluctuations.[50] The SQI patterns can be readily visualized using the conductance (G) vs B oscillations under zero DC bias (Figure 4 c, d). Indeed, even though the finite temperature and large R_N prevent to directly measure the critical current, the conductance is still mostly proportional to I_c when I_c is on the order of $2ek_BT/\hbar$, according to simulations based on the Resistively and Capacitively Shunted Junction (RCSJ) model (Figure S5).

A strong suppression of the supercurrent is observed when the Fermi level is placed below the SL induced band gap (especially clear for D2 at $0.98n_s$ in Figure 4c). Surprisingly, as the Fermi level enters the gap ($0.99n_s$), edge conduction immediately dominates the transport behavior of the t-BLG JJ and the SQUID pattern is observed. As the conduction bands are populated ($1.00n_s$ and above), additional contributions overlay with the SQUID pattern and the intensity of the center lobe becomes increasingly dominant because of the onset of bulk conduction. Moreover, the period of the SQI pattern gradually decreases from 1.88 mT down to 0.70 mT. The rapid change of the conduction channels and overall dependence on the carrier concentration further indicates that the behavior is intrinsic to the band structure of t-BLG around n_s. For instance, increasing the carrier density from $0.98n_s$ to $0.99n_s$ corresponds to adding ~80 electrons to the device. Because the resistance at $0.98n_s$ and $0.99n_s$ is almost identical, we can exclude edge conduction mechanisms unrelated to the moiré bands such as trivial dangling bond states. In fact, if such edge conduction channels were present but buried by bulk conduction at higher carrier concentration, they would show up at fillings with large resistance just outside the SL gap (e.g., $0.98n_s$). However, the drastic change observed around n_s is consistent with the filling of topological edge states in the SL

https://doi.org/10.1021/acs.nanolett.2c01481
Nano Lett. 2022, 22, 6186−6193

gap. Moreover, edge modes that would show up only at the Dirac point, such as monolayer zigzag edge states, can also be ruled out.

A similar overall evolution is observed for D3 (Figure 4d), with a Fraunhofer pattern period of 1.04 mT away from the gap ($1.33n_s$) and a SQUID pattern period of 2.80 mT at $1.03-1.04n_s$ (ratio of 2.7). The absence of irregularities in the period of the interference patterns for D3, together with the larger resistance suggest that this device has no inhomogeneities and thus displays the intrinsic behavior of t-BLG. Furthermore, a similar behavior is observed on the hole side SL gap due to electron−hole symmetry (Figure S4). We note that the SQUID SQI is observed slightly away from the insulating peak, which may be due to the large resistance of D3. In fact, the edge conduction may contribute to the decrease in the resistance as the Fermi level enters the band gap.

In summary, we revealed the presence of edge dominated conduction within the superlattice induced band gaps of t-BLG using superconducting quantum interference to probe the current distribution in Josephson junctions. Highly homogeneous t-BLG JJs display pure edge conduction when the Fermi level is placed inside the band gap. Moreover, the absence of edge conduction at fillings just below the superlattice band gap confirms that the edge channels are associated with electronic states located inside the band gaps, which strongly suggests their topological origin. An increase in the period of the interference patterns was observed at and near the electron and hole superlattice band gaps in devices with high twist angle homogeneity. The origin of the anomalous periodicity requires further investigations. These results highlight the nontrivial topology of the moiré bands of twisted bilayer graphene and will stimulate further experimental and theoretical investigations to determine the exact nature of the edge states and assess the presence of higher-order topology in t-BLG.

■ ASSOCIATED CONTENT

Supporting Information

The Supporting Information is available free of charge at https://pubs.acs.org/doi/10.1021/acs.nanolett.2c01481.

Methods (device fabrication, superconducting quantum interferometry measurements, supercurrent reconstruction, band structure calculations, RCSJ simulations, twist-angle, carrier concentration, and device mobility estimation), relation between sheet resistance, SL peak half-width and twist angle homogeneity, interference patterns for D1, interference pattern in the negative B range for D2, periodicity of the interference patterns, interference pattern for device D3 near the SL band gaps, use of $G(B)$ to visualize $I_c(B)$ (PDF)

■ AUTHOR INFORMATION

Corresponding Authors

Matthieu Fortin-Deschênes − *Department of Electrical Engineering, Yale University, New Haven, Connecticut 06511, United States*; Email: matthieu.fortin-deschenes@yale.edu

Yan-Feng Zhou − *Department of Physics, The University of Texas at Dallas, Richardson, Texas 7508, United States*; Email: yanfeng.zhou@utdallas.edu

Xu Du − *Department of Physics and Astronomy, Stony Brook University, Stony Brook, New York 11794, United States*; orcid.org/0000-0001-5610-2338; Email: xu.du@stonybrook.edu

Authors

Rui Pu − *Department of Physics and Astronomy, Stony Brook University, Stony Brook, New York 11794, United States*

Chao Ma − *Department of Electrical Engineering, Yale University, New Haven, Connecticut 06511, United States*; orcid.org/0000-0002-2879-3239

Patrick Cheung − *Department of Physics, The University of Texas at Dallas, Richardson, Texas 7508, United States*

Kenji Watanabe − *Research Center for Functional Materials, National Institute for Materials Science, Tsukuba 305-0044, Japan*; orcid.org/0000-0003-3701-8119

Takashi Taniguchi − *International Center for Materials Nanoarchitectonics, National Institute for Materials Science, Tsukuba 305-0044, Japan*; orcid.org/0000-0002-1467-3105

Fan Zhang − *Department of Physics, The University of Texas at Dallas, Richardson, Texas 7508, United States*; orcid.org/0000-0003-4623-4200

Fengnian Xia − *Department of Electrical Engineering, Yale University, New Haven, Connecticut 06511, United States*; orcid.org/0000-0001-5176-368X

Complete contact information is available at: https://pubs.acs.org/10.1021/acs.nanolett.2c01481

Notes

The authors declare no competing financial interest.

■ ACKNOWLEDGMENTS

M.F.-D. acknowledges support from the Natural Sciences and Engineering Research Council of Canada (NSERC) and Fonds de recherche du Québec (FRQNT). M.F.-D. and F.X. acknowledge the partial support from Government of Israel. X.D. acknowledges support from the National Science Foundation (NSF) under award DMR-1808491. Y.-F.Z. and F.Z. acknowledge support from the Army Research Office under grant W911NF-18-1-0416 and the NSF under grant DMR-2105139 through the CMP program. P.C. and F.Z. acknowledge support from the NSF under grants DMR-1945351 through the CAREER program and DMR-1921581 through the DMREF program. K.W. and T.T. acknowledge support from JSPS KAKENHI (Grants 19H05790, 20H00354, and 21H05233).

■ REFERENCES

(1) Rong, Z. Y.; Kuiper, P. Electronic Effects in Scanning Tunneling Microscopy: Moiré Pattern on a Graphite Surface. *Phys. Rev. B* **1993**, *48* (23), 17427−17431.

(2) Bistritzer, R.; MacDonald, A. H. Moiré Bands in Twisted Double-Layer Graphene. *Proc. Natl. Acad. Sci. U. S. A.* **2011**, *108* (30), 12233−12237.

(3) Kim, K.; Yankowitz, M.; Fallahazad, B.; Kang, S.; Movva, H. C. P.; Huang, S.; Larentis, S.; Corbet, C. M.; Taniguchi, T.; Watanabe, K.; et al. Van Der Waals Heterostructures with High Accuracy Rotational Alignment. *Nano Lett.* **2016**, *16* (3), 1989−1995.

(4) Kim, K.; DaSilva, A.; Huang, S.; Fallahazad, B.; Larentis, S.; Taniguchi, T.; Watanabe, K.; LeRoy, B. J.; MacDonald, A. H.; Tutuc, E. Tunable Moiré Bands and Strong Correlations in Small-Twist-Angle Bilayer Graphene. *Proc. Natl. Acad. Sci. U. S. A.* **2017**, *114* (13), 3364−3369.

(5) Lau, C. N.; Bockrath, M. W.; Mak, K. F.; Zhang, F. Reproducibility in the Fabrication and Physics of Moiré Materials. *Nature* **2022**, *602* (7895), 41−50.
(6) Alexeev, E. M.; Ruiz-Tijerina, D. A.; Danovich, M.; Hamer, M. J.; Terry, D. J.; Nayak, P. K.; Ahn, S.; Pak, S.; Lee, J.; Sohn, J. I.; et al. Resonantly Hybridized Excitons in Moiré Superlattices in Van Der Waals Heterostructures. *Nature* **2019**, *567* (7746), 81.
(7) Jin, C.; Regan, E. C.; Yan, A.; Iqbal Bakti Utama, M.; Wang, D.; Zhao, S.; Qin, Y.; Yang, S.; Zheng, Z.; Shi, S.; et al. Observation of Moiré Excitons in Wse 2/Ws 2 Heterostructure Superlattices. *Nature* **2019**, *567* (7746), 76.
(8) Seyler, K. L.; Rivera, P.; Yu, H.; Wilson, N. P.; Ray, E. L.; Mandrus, D. G.; Yan, J.; Yao, W.; Xu, X. Signatures of Moiré-Trapped Valley Excitons in Mose 2/Wse 2 Heterobilayers. *Nature* **2019**, *567* (7746), 66.
(9) Tran, K.; Moody, G.; Wu, F.; Lu, X.; Choi, J.; Kim, K.; Rai, A.; Sanchez, D. A.; Quan, J.; Singh, A.; et al. Evidence for Moiré Excitons in Van Der Waals Heterostructures. *Nature* **2019**, *567* (7746), 71.
(10) Yu, H.; Liu, G.-B.; Tang, J.; Xu, X.; Yao, W. Moiré Excitons: From Programmable Quantum Emitter Arrays to Spin-Orbit−Coupled Artificial Lattices. *Science Advances* **2017**, *3* (11), No. e1701696.
(11) Moon, P.; Koshino, M. Energy Spectrum and Quantum Hall Effect in Twisted Bilayer Graphene. *Phys. Rev. B* **2012**, *85* (19), 195458.
(12) Cao, Y.; Luo, J. Y.; Fatemi, V.; Fang, S.; Sanchez-Yamagishi, J. D.; Watanabe, K.; Taniguchi, T.; Kaxiras, E.; Jarillo-Herrero, P. Superlattice-Induced Insulating States and Valley-Protected Orbits in Twisted Bilayer Graphene. *Phys. Rev. Lett.* **2016**, *117* (11), 116804.
(13) Codecido, E.; Wang, Q.; Koester, R.; Che, S.; Tian, H.; Lv, R.; Tran, S.; Watanabe, K.; Taniguchi, T.; Zhang, F.; et al. Correlated Insulating and Superconducting States in Twisted Bilayer Graphene Below the Magic Angle. *Science Advances* **2019**, *5* (9), No. eaaw9770.
(14) Yankowitz, M.; Chen, S.; Polshyn, H.; Zhang, Y.; Watanabe, K.; Taniguchi, T.; Graf, D.; Young, A. F.; Dean, C. R. Tuning Superconductivity in Twisted Bilayer Graphene. *Science* **2019**, *363* (6431), 1059−1064.
(15) Cao, Y.; Fatemi, V.; Demir, A.; Fang, S.; Tomarken, S. L.; Luo, J. Y.; Sanchez-Yamagishi, J. D.; Watanabe, K.; Taniguchi, T.; Kaxiras, E.; et al. Correlated Insulator Behaviour at Half-Filling in Magic-Angle Graphene Superlattices. *Nature* **2018**, *556* (7699), 80−84.
(16) Cao, Y.; Fatemi, V.; Fang, S.; Watanabe, K.; Taniguchi, T.; Kaxiras, E.; Jarillo-Herrero, P. Unconventional Superconductivity in Magic-Angle Graphene Superlattices. *Nature* **2018**, *556* (7699), 43−50.
(17) Sharpe, A. L.; Fox, E. J.; Barnard, A. W.; Finney, J.; Watanabe, K.; Taniguchi, T.; Kastner, M. A.; Goldhaber-Gordon, D. Emergent Ferromagnetism near Three-Quarters Filling in Twisted Bilayer Graphene. *Science* **2019**, *365* (6453), 605−608.
(18) Hejazi, K.; Liu, C.; Shapourian, H.; Chen, X.; Balents, L. Multiple Topological Transitions in Twisted Bilayer Graphene near the First Magic Angle. *Phys. Rev. B* **2019**, *99* (3), 035111.
(19) Ahn, J.; Park, S.; Yang, B.-J. Failure of Nielsen-Ninomiya Theorem and Fragile Topology in Two-Dimensional Systems with Space-Time Inversion Symmetry: Application to Twisted Bilayer Graphene at Magic Angle. *Physical Review X* **2019**, *9* (2), 021013.
(20) Po, H. C.; Zou, L.; Senthil, T.; Vishwanath, A. Faithful Tight-Binding Models and Fragile Topology of Magic-Angle Bilayer Graphene. *Phys. Rev. B* **2019**, *99* (19), 195455.
(21) Koshino, M. Band Structure and Topological Properties of Twisted Double Bilayer Graphene. *Phys. Rev. B* **2019**, *99* (23), 235406.
(22) Song, Z.; Wang, Z.; Shi, W.; Li, G.; Fang, C.; Bernevig, B. A. All Magic Angles in Twisted Bilayer Graphene Are Topological. *Phys. Rev. Lett.* **2019**, *123* (3), 036401.
(23) Wang, Z.-H.; Xu, F.; Li, L.; Lü, R.; Wang, B.; Chen, W.-Q. One-Dimensional Topological Superconductivity at the Edges of Twisted Bilayer Graphene Nanoribbons. *Phys. Rev. B* **2019**, *100* (9), 094531.
(24) Park, M. J.; Kim, Y.; Cho, G. Y.; Lee, S. Higher-Order Topological Insulator in Twisted Bilayer Graphene. *Phys. Rev. Lett.* **2019**, *123* (21), 216803.
(25) Ma, C.; Wang, Q.; Mills, S.; Chen, X.; Deng, B.; Yuan, S.; Li, C.; Watanabe, K.; Taniguchi, T.; Du, X.; et al. Moiré Band Topology in Twisted Bilayer Graphene. *Nano Lett.* **2020**, *20* (8), 6076−6083.
(26) Liu, B.; Xian, L.; Mu, H.; Zhao, G.; Liu, Z.; Rubio, A.; Wang, Z. F. Higher-Order Band Topology in Twisted Moiré Superlattice. *Phys. Rev. Lett.* **2021**, *126* (6), 066401.
(27) Wu, S.; Zhang, Z.; Watanabe, K.; Taniguchi, T.; Andrei, E. Y. Chern Insulators, Van Hove Singularities and Topological Flat Bands in Magic-Angle Twisted Bilayer Graphene. *Nat. Mater.* **2021**, *20* (4), 488−494.
(28) Zhang, F.; MacDonald, A. H.; Mele, E. J. Valley Chern Numbers and Boundary Modes in Gapped Bilayer Graphene. *Proc. Natl. Acad. Sci. U. S. A.* **2013**, *110* (26), 10546−10551.
(29) Ju, L.; Shi, Z.; Nair, N.; Lv, Y.; Jin, C.; Velasco, J.; Ojeda-Aristizabal, C.; Bechtel, H. A.; Martin, M. C.; Zettl, A.; et al. Topological Valley Transport at Bilayer Graphene Domain Walls. *Nature* **2015**, *520* (7549), 650−655.
(30) Huang, S.; Kim, K.; Efimkin, D. K.; Lovorn, T.; Taniguchi, T.; Watanabe, K.; MacDonald, A. H.; Tutuc, E.; LeRoy, B. J. Topologically Protected Helical States in Minimally Twisted Bilayer Graphene. *Phys. Rev. Lett.* **2018**, *121* (3), 037702.
(31) Yao, Q.; Chen, X.; van Bremen, R.; Sotthewes, K.; Zandvliet, H. J. W. Singularities and Topologically Protected States in Twisted Bilayer Graphene. *Appl. Phys. Lett.* **2020**, *116* (1), 011602.
(32) Verbakel, J. D.; Yao, Q.; Sotthewes, K.; Zandvliet, H. J. W. Valley-Protected One-Dimensional States in Small-Angle Twisted Bilayer Graphene. *Phys. Rev. B* **2021**, *103* (16), 165134.
(33) Dynes, R. C.; Fulton, T. A. Supercurrent Density Distribution in Josephson Junctions. *Phys. Rev. B* **1971**, *3* (9), 3015−3023.
(34) Allen, M. T.; Shtanko, O.; Fulga, I. C.; Akhmerov, A. R.; Watanabe, K.; Taniguchi, T.; Jarillo-Herrero, P.; Levitov, L. S.; Yacoby, A. Spatially Resolved Edge Currents and Guided-Wave Electronic States in Graphene. *Nat. Phys.* **2016**, *12* (2), 128−133.
(35) Wang, L.; Meric, I.; Huang, P. Y.; Gao, Q.; Gao, Y.; Tran, H.; Taniguchi, T.; Watanabe, K.; Campos, L. M.; Muller, D. A.; et al. One-Dimensional Electrical Contact to a Two-Dimensional Material. *Science* **2013**, *342* (6158), 614−617.
(36) Rosenberger, M. R.; Chuang, H.-J.; McCreary, K. M.; Hanbicki, A. T.; Sivaram, S. V.; Jonker, B. T. Nano-"Squeegee" for the Creation of Clean 2d Material Interfaces. *ACS Appl. Mater. Interfaces* **2018**, *10* (12), 10379−10387.
(37) Singh, V.; Schneider, B. H.; Bosman, S. J.; Merkx, E. P. J.; Steele, G. A. Molybdenum-Rhenium Alloy Based High-Q Superconducting Microwave Resonators. *Appl. Phys. Lett.* **2014**, *105* (22), 222601.
(38) Zhu, M. J.; Kretinin, A. V.; Thompson, M. D.; Bandurin, D. A.; Hu, S.; Yu, G. L.; Birkbeck, J.; Mishchenko, A.; Vera-Marun, I. J.; Watanabe, K.; et al. Edge Currents Shunt the Insulating Bulk in Gapped Graphene. *Nat. Commun.* **2017**, *8* (1), 14552.
(39) Kononov, A.; Abulizi, G.; Qu, K.; Yan, J.; Mandrus, D.; Watanabe, K.; Taniguchi, T.; Schönenberger, C. One-Dimensional Edge Transport in Few-Layer Wte2. *Nano Lett.* **2020**, *20* (6), 4228−4233.
(40) Ke, C. T.; Draelos, A. W.; Seredinski, A.; Wei, M. T.; Li, H.; Hernandez-Rivera, M.; Watanabe, K.; Taniguchi, T.; Yamamoto, M.; Tarucha, S.; et al. Anomalous Periodicity of Magnetic Interference Patterns in Encapsulated Graphene Josephson Junctions. *Physical Review Research* **2019**, *1* (3), 033084.
(41) de Vries, F. K.; Sol, M. L.; Gazibegovic, S.; Veld, R. L. M. o. h.; Balk, S. C.; Car, D.; Bakkers, E. P. A. M.; Kouwenhoven, L. P.; Shen, J. Crossed Andreev Reflection in Insb Flake Josephson Junctions. *Physical Review Research* **2019**, *1* (3), 032031.
(42) de Vries, F. K.; Timmerman, T.; Ostroukh, V. P.; van Veen, J.; Beukman, A. J. A.; Qu, F.; Wimmer, M.; Nguyen, B.-M.; Kiselev, A. A.; Yi, W.; et al. H/E Superconducting Quantum Interference through Trivial Edge States in Inas. *Phys. Rev. Lett.* **2018**, *120* (4), 047702.

https://doi.org/10.1021/acs.nanolett.2c01481
Nano Lett. 2022, 22, 6186−6193

(43) Heida, J. P.; van Wees, B. J.; Klapwijk, T. M.; Borghs, G. Nonlocal Supercurrent in Mesoscopic Josephson Junctions. *Phys. Rev. B* **1998**, *57* (10), R5618−R5621.
(44) Pribiag, V. S.; Beukman, A. J. A.; Qu, F.; Cassidy, M. C.; Charpentier, C.; Wegscheider, W.; Kouwenhoven, L. P. Edge-Mode Superconductivity in a Two-Dimensional Topological Insulator. *Nat. Nanotechnol.* **2015**, *10* (7), 593−597.
(45) Baxevanis, B.; Ostroukh, V. P.; Beenakker, C. W. J. Even-Odd Flux Quanta Effect in the Fraunhofer Oscillations of an Edge-Channel Josephson Junction. *Phys. Rev. B* **2015**, *91* (4), 041409.
(46) Houzet, M.; Meyer, J. S.; Badiane, D. M.; Glazman, L. I. Dynamics of Majorana States in a Topological Josephson Junction. *Phys. Rev. Lett.* **2013**, *111* (4), 046401.
(47) Lee, S.-P.; Michaeli, K.; Alicea, J.; Yacoby, A. Revealing Topological Superconductivity in Extended Quantum Spin Hall Josephson Junctions. *Phys. Rev. Lett.* **2014**, *113* (19), 197001.
(48) Lin, J.-X.; Zhang, Y.-H.; Morissette, E.; Wang, Z.; Liu, S.; Rhodes, D.; Watanabe, K.; Taniguchi, T.; Hone, J.; Li, J. I. A. Spin-Orbit−Driven Ferromagnetism at Half Moiré Filling in Magic-Angle Twisted Bilayer Graphene. *Science* **2022**, *375* (6579), 437−441.
(49) Little, W. A.; Parks, R. D. Observation of Quantum Periodicity in the Transition Temperature of a Superconducting Cylinder. *Phys. Rev. Lett.* **1962**, *9* (1), 9−12.
(50) Lee, P. A.; Stone, A. D. Universal Conductance Fluctuations in Metals. *Phys. Rev. Lett.* **1985**, *55* (15), 1622−1625.

https://doi.org/10.1021/acs.nanolett.2c01481
Nano Lett. 2022, 22, 6186−6193